

## Strathprints Institutional Repository

Scheurich, Frank and Brown, Richard (2013) *Modelling the aerodynamics of vertical-axis wind turbines in unsteady wind conditions*. Wind Energy, 16 (2). pp. 91-107. ISSN 1095-4244

Strathprints is designed to allow users to access the research output of the University of Strathclyde. Copyright © and Moral Rights for the papers on this site are retained by the individual authors and/or other copyright owners. You may not engage in further distribution of the material for any profitmaking activities or any commercial gain. You may freely distribute both the url (<http://strathprints.strath.ac.uk/>) and the content of this paper for research or study, educational, or not-for-profit purposes without prior permission or charge.

Any correspondence concerning this service should be sent to Strathprints administrator: <mailto:strathprints@strath.ac.uk>

# Modelling the Aerodynamics of Vertical-Axis Wind Turbines in Unsteady Wind Conditions

Frank Scheurich

University of Glasgow, Glasgow, UK

E-Mail: f.scheurich@aero.gla.ac.uk

Richard E. Brown

University of Strathclyde, Glasgow, UK

E-Mail: richard.brown@strath.ac.uk

Most numerical and experimental studies of the performance of vertical-axis wind turbines have been conducted with the rotors in steady, and thus somewhat artificial, wind conditions - with the result that turbine aerodynamics, under varying wind conditions, are still poorly understood. The Vorticity Transport Model has been used to investigate the aerodynamic performance and wake dynamics, both in steady and unsteady wind conditions, of three different vertical-axis wind turbines: one with a straight-bladed configuration, another with a curved-bladed configuration and another with a helically twisted configuration. The turbines with non-twisted blades are shown to be somewhat less efficient than the turbine with helically twisted blades when the rotors are operated at constant rotational speed in unsteady wind conditions. In steady wind conditions, the power coefficients that are produced by both the straight- and the curved-bladed turbines vary considerably within one rotor revolution because of the continuously varying angle of attack on the blades and, thus, the inherent unsteadiness in the blade aerodynamic loading. These variations are much larger, and thus far more significant, than those that are induced by the unsteadiness in the wind conditions.

## Nomenclature

$A$	swept area
$b$	blade span
$c$	chord length of the rotor blade
$C_P$	power coefficient, $P/\frac{1}{2}\rho AV^3$
$D_g$	gust length, $V_\infty/f_c$
$f_c$	characteristic fluctuation frequency
$F_n$	sectional force acting normal to the blade chord
$F_t$	sectional force acting tangential to the blade chord
$k_g$	reduced gust frequency, $2R/D_g$
$P$	power
$R$	reference radius of the rotor
$R_g$	Number of rotor revolutions per gust, $\lambda_{mean}/\pi k_g$
$Re$	blade (rotational) Reynolds number, $\Omega Rc/\nu$
$S$	vorticity source
$u$	flow velocity
$u_b$	flow velocity relative to the blade
$V$	(unsteady) wind speed, $V = V(t)$
$V_\infty$	(steady) wind speed, mean free stream velocity
$\Delta V$	unsteady component of the wind velocity, $V(t) - V_\infty$
$z$	coordinate; the z-axis is aligned with the rotational axis of the rotor
$\alpha$	angle of attack
$\lambda$	tip speed ratio, $\Omega R/V$
$\lambda_{mean}$	mean tip speed ratio, $\Omega R/V_\infty$
$\nu$	kinematic viscosity
$\psi$	azimuth
$\rho$	air density
$\omega$	vorticity
$\omega_b$	vorticity bound to the rotor blades
$\Omega$	angular velocity of the rotor

## 1. Introduction

Interest in the application of wind turbines for decentralised electricity generation within cities has increased considerably in recent years. The design of a wind turbine that operates efficiently within the urban environment poses a significant challenge, however, since the wind in the built environment is characterised by frequent and often rapid changes in direction and speed. In these wind conditions, vertical-axis wind turbines might offer several advantages over horizontal-axis wind turbines. This is because vertical-axis turbines do not require a yaw control system, whereas horizontal-axis wind turbines have to be rotated in order to track changes in wind direction. In addition, the gearbox and the generator of a vertical-axis turbine can be situated at the base of the turbine, thereby reducing the loads on the tower and facilitating the maintenance of the system. The principal advantage of these features of a vertical-axis configuration is to enable a somewhat more compact design that alleviates the material stress on the tower and requires fewer mechanical components compared to a horizontal-axis turbine.

Most experimental and numerical studies of the aerodynamic performance of vertical-axis wind turbines have been conducted with the rotors in *steady* wind conditions. This is either because of the inherent difficulties of wind tunnel experiments under unsteady wind conditions or because of the significant challenge that the accurate simulation of the aerodynamics of vertical-axis wind turbines - in either steady or unsteady wind conditions - poses to numerical modelling techniques. Field tests of full-scale turbine configurations are only partially instructive since they do not allow the various mechanisms that cause the unsteadiness in turbine behaviour to be isolated and studied independently. Detailed analyses of the blade aerodynamic loading and the performance of vertical-axis wind turbines when operated in an *unsteady* wind, and thus in conditions that are more representative of real-world operation, are therefore scarce in the literature. Nevertheless Kang et al. [1] and Kooiman and Tullis [2] have conducted experimental studies of vertical-axis wind turbines in varying wind conditions and McIntosh [3] has performed a numerical investigation of the two-dimensional aerodynamics of

an aerofoil in a planar, cyclic motion designed to emulate that of the mid-section of the blade of vertical-axis wind turbine. These studies suggest that the vertical-axis wind turbine is, potentially, well suited to wind conditions that are characterised by frequent and rapid changes in direction and speed.

The present paper contributes to the understanding of the aerodynamic behaviour of vertical-axis wind turbines when they are subject to temporal variations of wind speed. The Vorticity Transport Model developed by Brown [4], and extended by Brown and Line [5], has been used to investigate the aerodynamic performance and wake dynamics, both in steady and unsteady wind conditions, of three different vertical-axis wind turbines: one with a straight-bladed configuration, another with a curved-bladed configuration and another with a helically twisted configuration.

## 2. Computational Aerodynamics

The VTM models the aerodynamics of wind turbines by providing an accurate representation of the dynamics of the wake that is generated by the turbine rotor. An outline of the model is given below but the reader is referred to the original Refs. [4] and [5] for a more detailed description of the method. In the VTM, the time-dependent Navier-Stokes equations are discretised in three-dimensional finite-volume form using a structured Cartesian mesh within the fluid domain surrounding the turbine rotor. Under the assumption that the wake is incompressible, the Navier-Stokes equations can be cast into the vorticity-velocity form

$$\frac{\partial}{\partial t}\omega + u \cdot \nabla\omega - \omega \cdot \nabla u = S + \nu\nabla^2\omega \quad (1)$$

allowing the temporal evolution of the vorticity distribution  $\omega = \nabla \times u$  in the flow surrounding the rotor to be calculated. The various terms within the vorticity transport equation describe the changes in the vorticity field,  $\omega$ , with time at any point in space, as a function of the velocity field,  $u$ , and the viscosity,  $\nu$ . The vorticity source term,  $S$ , is used to account for the creation of vorticity at solid surfaces immersed within the fluid. The vorticity source term is determined as the sum of the temporal and spatial variations in the bound vorticity,  $\omega_b$ , on the turbine blades so that

$$S = -\frac{d}{dt}\omega_b + u_b\nabla \cdot \omega_b \quad (2)$$

The first term in Equation 2 represents the shed vorticity and the second term represents the trailed vorticity from the blade. The bound vorticity distribution on the blades of the rotor is modelled using an extension of lifting-line theory. The lifting-line approach has been appropriately modified by the use of two-dimensional experimental data in order to represent the real performance of any given airfoil. The effect of dynamic stall on the aerodynamic performance of the aerofoil is accounted for by using a semi-empirical dynamic stall model that is based on the model that was proposed by Leishman and Beddoes [6]. For calculations of full scale turbine aerodynamics, the assumption is usually made that the Reynolds number

within the computational domain is sufficiently high so that the equations governing the flow in the wake of the rotor may be solved in inviscid form, and thus that the viscosity  $\nu$  in Equation 1 can be set equal to zero. The numerical diffusion of vorticity within the flow field surrounding the wind turbine is kept at a very low level by using a Riemann solver based on the Weighted Average Flux method developed by Toro [7] to advance the advection term in Equation 1 through time. This approach permits many rotor revolutions to be captured without significant spatial smearing of the wake structure, in contrast to the performance of more conventional CFD techniques that are based on the pressure-velocity formulation of the Navier-Stokes equations. The wake does naturally dissipate with time, however, because of the inherent instability of the vortical structures of which it is composed.

The VTM was originally developed for simulating the flow field surrounding helicopters, but is an aerodynamic tool that is applicable also to the study of wind turbine rotors. Indeed, Scheurich, Fletcher and Brown [8] have compared VTM predictions against experimental measurements of the blade aerodynamic loading of a straight-bladed vertical-axis wind turbine that were made by Strickland, Smith and Sun [9]. Furthermore, Scheurich and Brown [10] have compared VTM predictions against experimental measurements of the power curve that were made by Penna [11] for a commercial vertical-axis wind turbine with blades that are helically twisted around the rotor axis. The very satisfactory agreement between VTM predictions and all these different and independent experimental measurements provides considerable confidence in the ability of the VTM to model accurately the aerodynamics of vertical-axis wind turbines.

### 3. Turbine Model

The geometry of each of the three vertical-axis wind turbines that are investigated in this study is illustrated in Figure 1. The blades of each turbine are separated by  $120^\circ$  azimuth. Starting from the straight-bladed configuration, shown in Figure 1(a), the radial location of each blade section was displaced using a hyperbolic cosine distribution in order to yield the troposkien shape of the curved-bladed configuration shown in Figure 1(b). The helically twisted configuration, shown in Figure 1(c), was then obtained by twisting the blades around the rotor axis. The blades of the straight- and curved-bladed configuration, and each individual section of the blades of the helically twisted configuration, are designed to have zero geometric pitch angle. In other words, the chord of each blade section is tangential to the local segment of the circle that is described by the trajectory of the blades. The maximum radius,  $R$ , of each rotor is at the mid-span of the reference blade ('blade 1') of the turbine, and is identical for each of the three different configurations. This radius is used as the reference radius of the rotor when presenting non-dimensional data for the performance of the turbine. The tip speed ratio,  $\lambda$ , is defined as the ratio between the circumferential velocity at the mid-span of the blade,  $\Omega R$ , and the wind speed,  $V$ . The key parameters of the rotor are summarised in Table 1 but the reader is referred to Ref. [12] for a more detailed description of these configurations. The orientation of the blades and the specification of the azimuth angle of the turbine with respect to the mid-span of the reference blade are shown in Figure 2.

The behaviour of the three different turbine configurations is studied both in steady and in unsteady wind conditions. An 'ideal' vertical-axis wind turbine would always operate at the tip speed ratio for which the maximum efficiency is obtained. This would be done by adjusting the rotational speed of the rotor, when the wind speed changes, in order to keep a constant tip speed ratio. This control strategy is generally very difficult to implement in practice because of the inertia of the rotor and the response time that is associated with any practical control system. In all the simulations that are presented in this paper, the rotational speed of the rotors was kept constant in order to isolate the aerodynamic effects that will be introduced



by the fluctuation in wind speed from the additional unsteady aerodynamic effects that will be introduced when the rotor accelerates or decelerates. This is consistent, in practical terms, with the behaviour of rotors where the rotational speed cannot be made to respond rapidly to changes in wind speed.

## 4. Turbine Performance in Steady Wind Conditions

Before the aerodynamic behaviour of vertical-axis wind turbines in unsteady wind conditions can be understood, it is important to understand first the aerodynamic performance of this type of rotor in steady wind conditions. The discussion presented here is necessarily brief but for a more detailed analysis of the blade aerodynamic loading, rotor performance and the structure of the wake that is produced by vertical-axis turbines in *steady* wind conditions, the reader is referred to the study carried out by Scheurich, Fletcher and Brown [12].

Figure 3 shows the variation with azimuth of the power coefficients that are produced by the straight- and curved-bladed configurations and the turbine with helically twisted blades over the range of operationally-relevant tip speed ratios. The three tip speed ratios for which data is presented are equivalent to high, moderate and low tip speed ratios within the range over which lift-driven vertical-axis wind turbines typically operate. The peak loading on the rotating blade of a non-twisted vertical-axis wind turbine occurs at  $90^\circ$  azimuth. This is because, with the blade at this azimuth position, the wind vector is perpendicular to the aerofoil chord, thereby producing a high angle of attack on the blade and, consequently, a high aerodynamic loading. The straight- and curved-bladed turbines produce a power coefficient that varies significantly within one turbine revolution; the three coherent peaks in the variation of the power coefficient close to  $90^\circ$ ,  $210^\circ$  and  $330^\circ$  azimuth reflect the peak in the aerodynamic loading of each individual blade as it rotates past  $90^\circ$  azimuth. Helical blade twist significantly reduces the oscillations in the power coefficient produced by a vertical-axis turbine, as shown in Figures 3(e) and (f). This is because of the more uniform distribution of blade area around the azimuth compared to a turbine with non-twisted blades and not because of any inherent reduction in the unsteadiness of the aerodynamic loading on the blades of this particular configuration.

Figure 4 shows the flow field surrounding the straight-bladed vertical-axis wind turbine in steady wind conditions. Figure 4(a) depicts the vorticity distribution on a vertical plane through the centre of the rotor. This plane contains the rotational axis of the rotor and is

aligned with the wind direction. The flow field is represented using contours of the component of vorticity perpendicular to the plane, thereby emphasising the vorticity that is trailed from the blades. The dark rendering corresponds to vorticity with a clockwise sense, and the light rendering to vorticity with a counter-clockwise sense of rotation. It is apparent that the mutual induction between the tip vortices that are produced by the blades of the turbine causes these structures to convect towards the centreline of the rotor. Interactions between the blades of the turbine and the tip vortices are clearly apparent downstream of the axis of rotation. These blade-vortex interactions cause localised impulsive perturbations to the blade aerodynamic loading, as shown later in this paper and analysed in detail in Refs. [8] and [12]. At some distance downstream of the rotor, the tip vortices that were trailed from the blades in the upwind and downwind portions of the rotor revolution are seen to interact and merge with each other to produce a highly disordered wake structure several rotor diameters downwind of the turbine.

Figure 4(b) shows the vorticity distribution on a horizontal plane through the centre of the rotor, emphasising the shed vorticity from the blades. The vorticity that is shed during the part of the revolution when the leading edges of the blades face the wind vector is somewhat smeared spatially. In contrast, compact individual vortices, rather than a set of smeared regions of vorticity, are produced during the portion of the revolution in which the blade moves with the wind, in other words, between  $90^\circ$  and  $270^\circ$  azimuth.

## 5. Turbine Performance in Unsteady Wind Conditions

By adopting the notation that was used by McIntosh [3], the variation in wind speed that is experienced by a vertical-axis wind turbine during a gust can be expressed in terms of a gust length

$$D_g = \frac{V_\infty}{f_c} \quad (3)$$

where  $V_\infty$  is the mean free stream velocity and  $f_c$  is the characteristic fluctuation frequency of the gust. The gust-induced unsteady aerodynamic effects that are encountered by a vertical-axis wind turbine with rotor radius,  $R$ , can then be characterised by a reduced gust frequency

$$k_g = \frac{2R}{D_g} = \frac{2Rf_c}{V_\infty} \quad (4)$$

Using the definition of the mean tip speed ratio,  $\lambda_{mean} = \Omega R/V_\infty$ , an expression for the number of rotor revolutions per gust can consequently be derived as

$$R_g = \frac{\lambda_{mean}}{\pi k_g} \quad (5)$$

Based on experimental measurements in an urban area, Bertényi, Wickins and McIntosh [13] estimated that the highest frequency of the fluctuations with meaningful energy content in urban wind conditions is of the order of 1Hz. In the present paper, results are presented for reduced gust frequencies  $k_g = 0.08$  and  $k_g = 0.74$ . A reduced gust frequency of  $k_g = 0.74$  would correspond, for example, to conditions in which a generic urban wind turbine with radius 2m was operated at a mean wind speed of 5.4m/s and encountered a gust with a characteristic fluctuation frequency of 1Hz. This would thus correspond to the severest operating conditions that this turbine would be likely to encounter in the urban environment.

In the VTM simulations presented below, the free stream velocity was varied sinusoidally around a mean velocity that gives a tip speed ratio of  $\lambda_{mean} = 3.5$ . The reduced gust frequencies give  $R_g = 14$  and  $R_g = 1.5$ , respectively. The behaviour of each of the three different turbines is compared when the sinusoidal variation of the free stream velocity has two different amplitudes:

$\Delta V/V_\infty = \pm 0.1$  and  $\Delta V/V_\infty = \pm 0.3$ . The assumption is made, within all the simulations presented below, that the gust field has infinite spatial extent.

## 5.1 Power Coefficient

Figure 5 shows the variation of the power coefficients that are produced by the three different turbines in unsteady wind conditions with  $R_g = 14$ . Data is presented for fourteen rotor revolutions in order to show the behaviour of the turbine over one complete gust period. The instantaneous power coefficient is based on the instantaneous wind speed and is presented for the corresponding instantaneous tip speed ratio. The mean power coefficient that is produced by each turbine configuration in steady wind conditions is shown for comparison along with ‘error bars’ that denote the variation of the power coefficient over each turbine revolution in steady wind, as described in Section 4 of this paper. The variation of the power coefficients produced by the turbines when subjected to the gust with  $k_g = 0.08$  is almost identical to that which would be produced in equivalent steady wind conditions. Indeed, it can be inferred from the data that when the turbine is exposed to a gust with such a low reduced frequency, its response is essentially quasi-steady.

Figure 6 shows the variation of the power coefficients that are produced by the turbines in unsteady wind conditions with  $R_g = 1.5$ . Although the period of the gust, under these conditions, is equal to 1.5 rotor revolutions, data is presented for three rotor revolutions - this is the number of rotor revolutions that must elapse in order for the turbine and the gust to return into phase. For  $\Delta V/V_\infty = \pm 0.1$ , the aerodynamic behaviour of the turbines can again be inferred to be essentially quasi-steady since no significant deviation is apparent from the range of variations of the power coefficients that are produced by the turbines under steady wind conditions at the same tip speed ratio. Increasing the amplitude of the sinusoidal variation of the free stream velocity, however, results in small but notable deviations from the quasi-steady behaviour of each turbine. Importantly, the variation of the power coefficients that is caused by the continuous change in angle of attack on the blades as they revolve is far more significant than those that are induced by the unsteadiness in the wind conditions. This observation is

described in more detail below.

A close-up of the variation of the power coefficient of each rotor when operated in unsteady wind conditions with  $R_g = 1.5$  and for  $\Delta V/V_\infty = \pm 0.3$  is shown in Figure 7 along with the temporal variation of the wind speed. The behaviour of the power coefficients in unsteady wind conditions is characterised by a hysteresis loop, indicated by the arrows in Figures 7(a), (b) and (c). The three dominant peaks per rotor revolution that characterise the variation of the power coefficients in steady wind conditions are still apparent, however. Interestingly, of the three turbines, the helically twisted configuration exhibits the highest relative deviation of the power coefficient in unsteady wind conditions from that in steady wind conditions. The amplitude of the variation of the power coefficient produced by the helically twisted configuration in unsteady wind conditions is much smaller, however, than that produced by either the straight- or the curved-bladed turbines.

As alluded to earlier, the ‘ideal’ vertical-axis wind turbine would maintain its tip speed ratio at that for maximum power by adjusting its rotational speed to match any changes in wind speed. Since the rotational speed of the turbines in this study was kept constant as the wind speed was varied the mean power coefficients that they produce can be expected to be smaller than those obtained at their optimum tip speed ratio. Figure 8 shows the mean power coefficient that is produced by each turbine in unsteady wind conditions as a percentage of that generated by an ‘ideal’ turbine operating at constant tip speed ratio. In other words, the figure indicates the loss that would be experienced by a ‘real’ turbine that has an inertia that is too high or a response time that is too long to adjust the rotational speed of the rotor to variations in the wind speed. The gust frequency has only a very small effect on the deviation of the power coefficient from the optimum value. Interestingly, Figure 8 shows that, at the lower amplitude of the sinusoidal variation of the wind speed that was investigated, almost 100% of the mean power coefficient of the ‘ideal’ turbine is obtained. Only at higher amplitudes of the sinusoidally varying wind speed do notable losses in the mean power coefficients occur for a rotor that operates at a fixed rotational speed in unsteady wind conditions.

Interestingly, the straight- and curved-bladed configurations exhibit greater losses in per-

formance than does the helically twisted configuration. This can be explained once it is realised that the variation of the power coefficient with tip speed ratio of either the straight- or curved-bladed turbines has a steeper gradient than the helically twisted configuration at mid-operating range, as shown in Figures 5 and 6 for steady wind conditions. Although the key rotor parameters of the three turbines are identical, the difference in their aerodynamic design leads, naturally, to different shapes of the power curves and thus to different absolute values of their power coefficients even if they are operated at the same tip speed ratio. The smaller gradient in the variation of the power coefficient produced by the helically-twisted configuration is a result of the fact that each individual section of its blades, due to a carefully chosen combination of blade curvature and twist, achieves its highest aerodynamic performance at a slightly different tip speed ratio. Thereby, the sudden drop, that is apparent in the  $C_P - \lambda$  curves of the non-twisted configurations when the tip speed ratio is different from the one at which the maximum power coefficient is produced, is avoided. It can thus be concluded that a turbine that features a steep gradient in its variation of power coefficient with tip speed ratio is more prone to power losses if the rotor speed is kept constant in unsteady wind conditions than a turbine that features a lower gradient in its  $C_P - \lambda$  curve.

It should be noted that the maximum efficiency achieved by a vertical-axis wind turbine, and the shape of the  $C_P - \lambda$  curve, depends on various parameters, such as the ratio between the blade chord and the rotor radius, as shown by Paraschivoiu [14, p. 71ff.] amongst others. It thus can not be concluded that the supremacy of the helically twisted design shown in the results presented here exists for all meaningful rotor parameters. In other words, it is conceivable that the  $C_P - \lambda$  curve of a turbine with suitably designed non-twisted blades could be as shallow as that produced by the helically twisted configuration. A parametric study with the aim of optimising the design of the non-twisted turbines was beyond the scope of the present investigation, however, given that the objective was simply to analyse the fundamental, and thus somewhat qualitative, differences in performance between straight- and curved-bladed turbines and helically twisted configurations.

## 5.2 Blade Aerodynamic Loading

The effect of unsteady wind conditions on the performance of the three different vertical-axis wind turbines is revealed in more detail by analysing the aerodynamic loading on the blades of the rotors. Figure 9 shows the aerodynamic angle of attack and the sectional normal and tangential forces that are generated at two different locations along the reference blade of the straight-bladed vertical-axis wind turbine during the three rotor revolutions that correspond to a single gust cycle. The figure shows a comparison between the angle of attack and the sectional forces that are produced in unsteady wind conditions and those generated in steady wind conditions. The forces are non-dimensionalised by the instantaneous wind speed in Figures 9(c) and (d), whereas Figures 9(e) and (f) show forces that are non-dimensionalised by the mean wind speed. The first set of curves are useful in order to compare qualitatively the blade aerodynamic loading produced in unsteady wind conditions to that produced in steady wind conditions, while the second set of curves provides a better gauge of the loads that are transmitted into the structure of the turbine.

In steady wind conditions, the variation of the angle of attack, and the variation of the sectional aerodynamic loading, features a peak close to  $90^\circ$  azimuth in each revolution. These peaks are the origin of the distinct peaks in the variation of the power coefficient that were shown in Figure 3(a). When the rotor is operated in steady wind conditions, both the angle of attack and the sectional forces show impulsive perturbations near to the tip of the blade as they rotate past  $270^\circ$  azimuth. These impulsive perturbations are induced by interactions between the blade and a region of concentrated vorticity in the wake of the turbine that consists, predominantly, of vorticity that was trailed in previous revolutions, as shown in Figure 4(a).

In unsteady wind conditions, the sectional angle of attack and the sectional loading show comparable features to those observed in steady wind conditions - for instance, the dominant peak close to  $90^\circ$  azimuth in each revolution and the perturbations due to blade-vortex interactions are still evident. As one might expect, the azimuthal variation of sectional forces and the angle of attack differs from rotor revolution to rotor revolution when the turbine is



operated in unsteady conditions. Interestingly, interactions of different strength between the blade and the tip vortices, reflected in different magnitudes of the blade aerodynamic loading close to  $270^\circ$  and  $630^\circ$  azimuth, occur within the first two rotor revolutions when the turbine is operated in unsteady wind conditions. Any significant perturbations to the angle of attack and the sectional aerodynamic loading on the blade are absent during the third revolution, close to  $990^\circ$  azimuth, however. This will be explained in the following section in terms of the vorticity distribution within the wake that is produced by the rotor in unsteady wind conditions.

### 5.3 Wake Structure

The flow field that surrounds the straight-bladed turbine in steady wind conditions was shown in Figures 4(a) and (b) by visualising the vorticity distribution on vertical and horizontal planes that are immersed within the wake of the rotor. Following the same approach the wake that is generated by the straight-bladed turbine in unsteady wind conditions is shown in Figures 10 and 11. The evolution of the wake is illustrated over the three rotor revolutions that correspond to a single gust period in steps of  $90^\circ$  azimuth. Figure 12 shows the three-dimensional flow field that surrounds the rotor, over three rotor revolutions in steps of  $360^\circ$  azimuth, by plotting a surface within the wake on which the vorticity has constant magnitude.

The behaviour of the wake reflects the periodic variation of the wind speed that was applied to the turbine. As a result of the oscillations in the onset wind speed, the distances between the individual tip vortices within the wake vary along its length, as can be seen clearly in Figures 10(a), (e) and (i). The reason for the presence of significant perturbations to the sectional angle of attack and the sectional loading on the blade during the first and second rotor revolution but not during the third revolution (see Figure 9) is revealed in the vorticity distribution in the wake that is depicted in Figures 10(d), (h) and (l). The uneven spacing between the tip vortices that is induced by the variation of onset wind speed allows the blade, within the third revolution, to pass through the wake without significant interaction with a tip vortex. This is not the case during the first and second revolutions, where the more dense distribution of tip vortices within the wake inevitably results in stronger blade-vortex

interactions. Downstream of the rotor, the effects of the mutual interactions between the tip vortices that are trailed in the upwind portion of the rotor revolution and those that are trailed in the downwind portion of the revolution are apparent. These interactions yield patches of merged vorticity within the wake, and these features grow in spatial extent as they convect further downstream. Although similar regions of merged vorticity can also be observed within the flow field in steady wind conditions, as shown in Figure 4, the vorticity distribution within the wake that is produced by the rotor in unsteady wind conditions is somewhat more disordered. Comparable structures within the wake to those seen in the vertical plane can also be seen on the horizontal slice through the wake shown in Figure 11. Interestingly, Figure 11 shows the wake structure to possess significant lateral asymmetry - the regions of clumped vorticity exist predominantly on the side of the turbine on which the leading edges of the blades face the wind. This asymmetry results primarily because the vorticity that is shed during the portion of the rotor revolution when the leading edges of the blades face the wind, is stronger than that which is shed when the blade moves with the wind. This results in a stronger mutual interaction between the vortices during the portion of the rotor revolution when the leading edges of the blades face the wind and hence in a tendency for these vortices to clump into larger structures more quickly. The complexity of the three-dimensional wake that is generated by the rotor is clearly apparent in Figure 12 where the mutual interaction between the shed and the trailed vorticity from the blades causes the individual vortices to break up to form a complex system of interwoven vortex filaments several rotor diameters downstream of the turbine.

## 6. Conclusion

The Vorticity Transport Model has been used to investigate the aerodynamic behaviour of three different vertical-axis wind turbines in wind speeds that vary sinusoidally with time. The instantaneous tip speed ratio of a rotor that is operated at a constant rotational speed in unsteady wind conditions changes according to the varying free stream velocity and, thereby, deviates from the tip speed ratio at which the highest aerodynamic efficiency is obtained. The associated power loss becomes significant only when the amplitude of the oscillations in wind speed is high, whereas the frequency of the variation in wind speed is shown to have a minor effect for all practical urban wind conditions. The power loss experienced by turbines with non-twisted blades is higher than for a vertical-axis wind turbine that has curved blades that are helically twisted around the rotor axis. This is because the straight- and the curved-bladed turbines that were investigated have a variation of the power coefficient with tip speed ratio that exhibits a steeper gradient in mid-operating range than the turbine with helically twisted blades. Each blade section of the helically twisted configuration achieves its highest individual aerodynamic performance - if blade curvature and helical twist are carefully chosen - at a slightly different tip speed ratio which results in a lower gradient in the variation of the power coefficient with tip speed ratio, by comparison. In steady wind conditions, the power coefficients that are produced by both the straight- and the curved-bladed turbines vary considerably within one rotor revolution because of the continuous variation of the angle of attack on the blades and, thus, the inherent unsteadiness in the blade aerodynamic loading. These variations are shown to be larger, and thus far more significant, than those that are induced by the unsteadiness in the wind conditions.

## Acknowledgements

The authors would like to thank Tamás Bertényi from *Quiet Revolution Ltd.* for his useful comments during the course of this study.

## References

1. Kang IS, Ariyasu K, Hara Y, Hayashi T, Paraschivoiu, I. Characteristics of a straight-bladed vertical axis wind turbine in periodically varying wind. *EXPO World Conference on Wind Energy, Renewable Energy, Fuel Cell (WCWRF 2005), Hamamatsu, Japan, 2005.*
2. Kooiman, SJ, Tullis SW. Response of a vertical axis wind turbine to time varying wind conditions found within the urban environment. *Wind Engineering* 2005; **34**: 389–401.
3. McIntosh S. Wind energy for the built environment. *PhD Thesis.* Department of Engineering, University of Cambridge, UK, 2009.
4. Brown RE. Rotor wake modelling for flight dynamic simulation of helicopters. *AIAA Journal* 2000; **38**: 57–63.
5. Brown RE, Line AJ. Efficient high-resolution wake modelling using the vorticity transport equation. *AIAA Journal* 2005; **43**: 1434–1443.
6. Leishman JG, Beddoes TS. A semi-empirical model for dynamic stall. *Journal of the American Helicopter Society*, 1989; **34**, 3–17.
7. Toro E. A weighted average flux method for hyperbolic conservation laws. *Proceedings of the Royal Society of London, Series A: Mathematical and Physical Sciences* 1981; **423**: 401–418.
8. Scheurich F, Fletcher TM, Brown RE. Simulating the aerodynamic performance and wake dynamics of a vertical-axis wind turbine. *Wind Energy*, 2011; **14**: 159–177.
9. Strickland JH, Smith T, Sun K. A vortex model of the Darrieus turbine: an analytical and experimental study. *Sandia National Laboratories, USA, SAND81-7017*, June 1981.
10. Scheurich F, Brown RE. Effect of dynamic stall on the aerodynamics of vertical-axis wind turbines. *AIAA Journal*, accepted for publication, February 2011, in press.
11. Penna PJ. Wind tunnel tests of the Quiet Revolution Ltd. QR5 vertical axis wind turbine. *Institute for Aerospace Research, National Research Council Canada, Canada, LTR-AL-2008-0004*, January 2008.
12. Scheurich F, Fletcher TM, Brown RE. Effect of blade geometry on the aerodynamic loads produced by vertical-axis wind turbines. *Proceedings of the Institution of Mechanical Engineers, Part A, Journal of Power and Energy*, 2011; **225**: 327–341.
13. Bertényi T, Wickins C, McIntosh S. Enhanced energy capture through gust-tracking in the urban wind environment. AIAA-2010-1376. *48th AIAA Aerospace Sciences Meeting, Orlando, Florida, USA, 2010.*
14. Paraschivoiu I. Wind turbine design: with emphasis on Darrieus concept. Polytechnic International Press, 2002.

Table 1: Rotor parameters.

---

---

Number of blades	3
Aerofoil section	NACA 0015
Blade Reynolds number at blade mid-span	800,000
Chord-to-radius ratio at mid-span	0.115
Aspect ratio	26

---

---

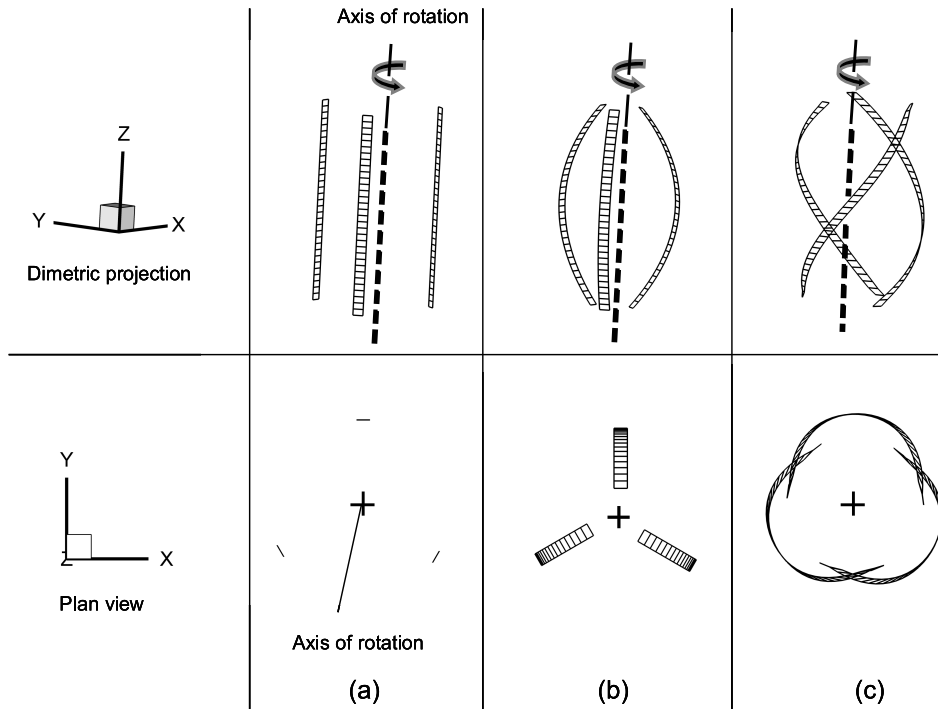


Figure 1: Geometry of the vertical-axis wind turbines with (a) straight, (b) curved, and (c) helically twisted blades.

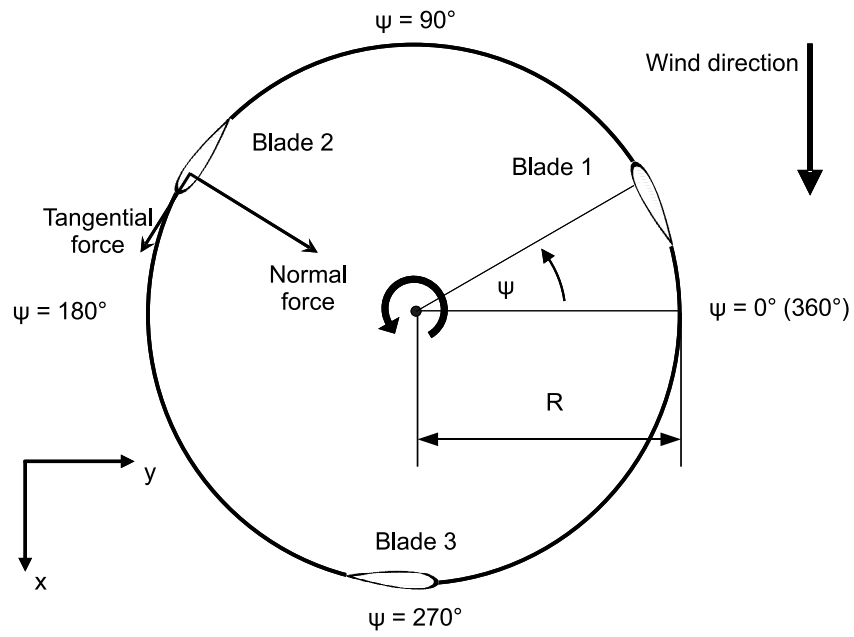
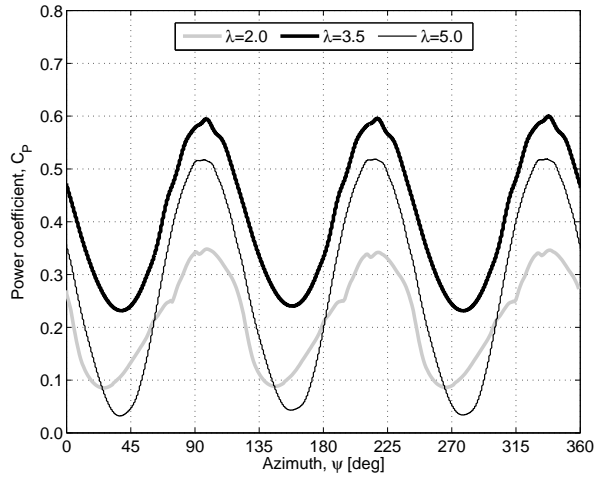
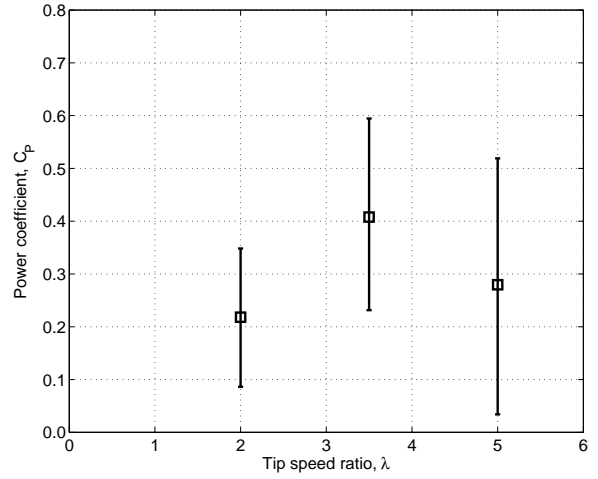


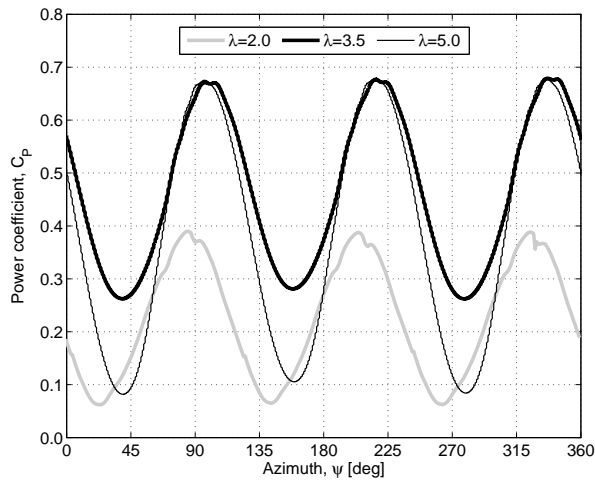
Figure 2: *Diagram showing the wind direction, the definition of rotor azimuth and direction of positive normal and tangential forces, as well as the relative positions of the rotor blades.*



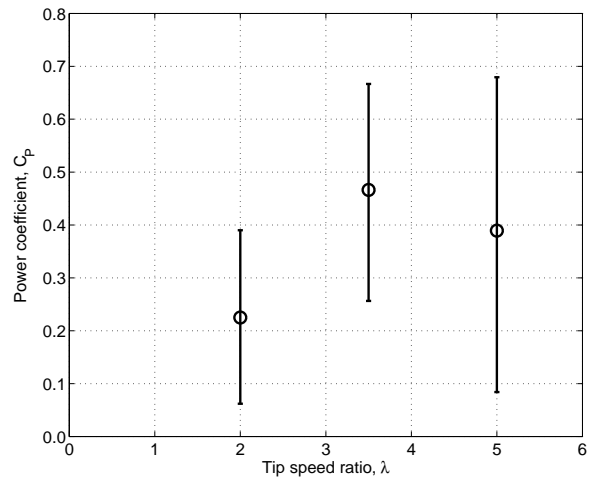
(a) *straight – bladed*



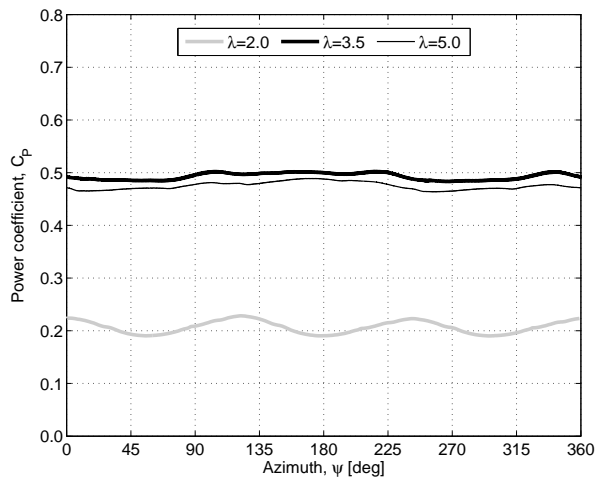
(b) *straight – bladed*



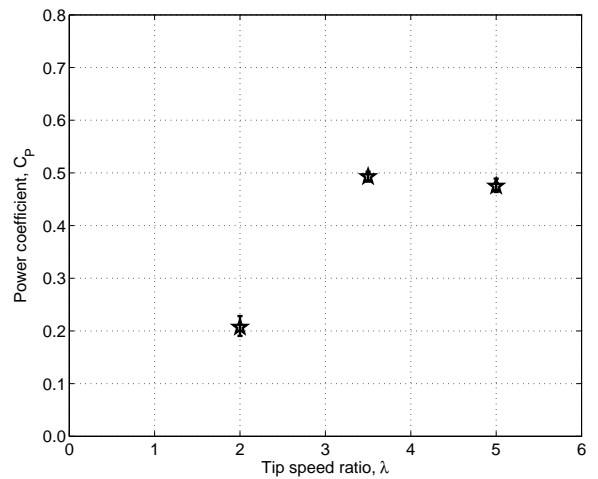
(c) *curved – bladed*



(d) *curved – bladed*



(e) *helically twisted*



(f) *helically twisted*

Figure 3: VTM-predicted variation of the mean power coefficients for the straight-bladed and curved-bladed turbine and the turbine with helically twisted blades in **steady** wind conditions. Error bars in subfigures (b), (d) and (f) denote the variation of the power coefficient during one rotor revolution.



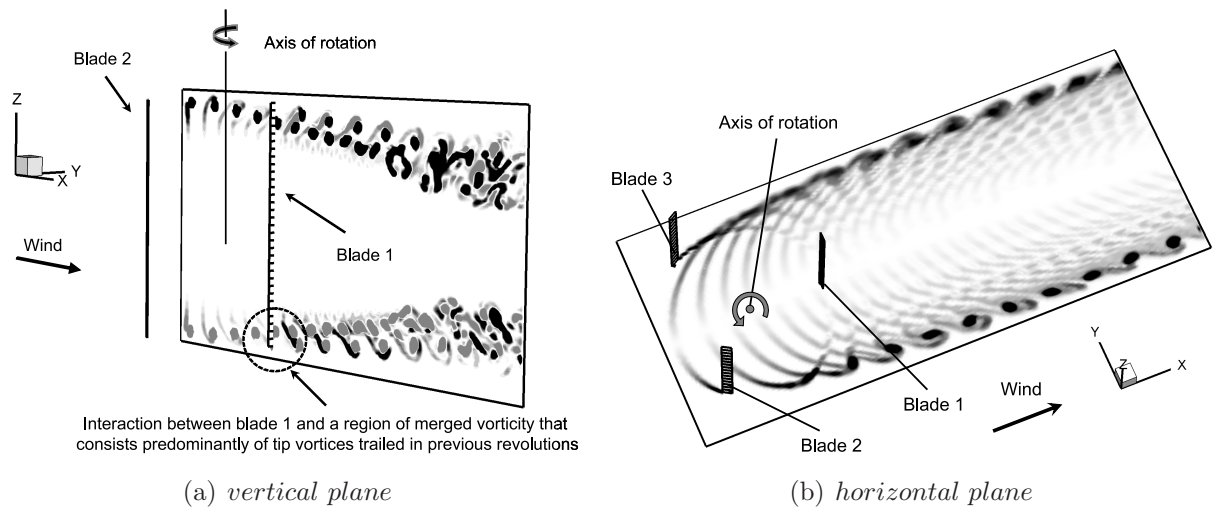
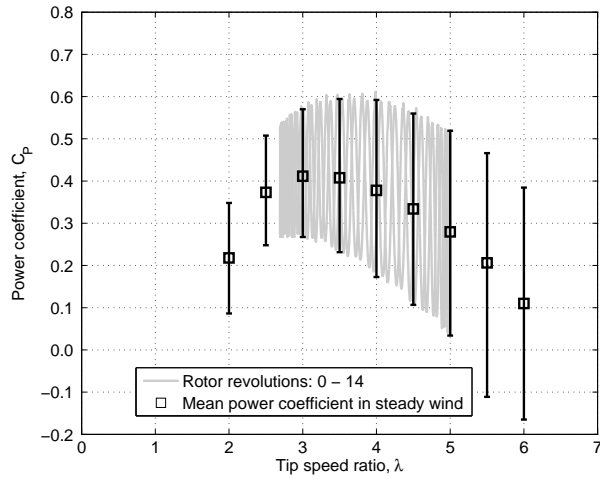
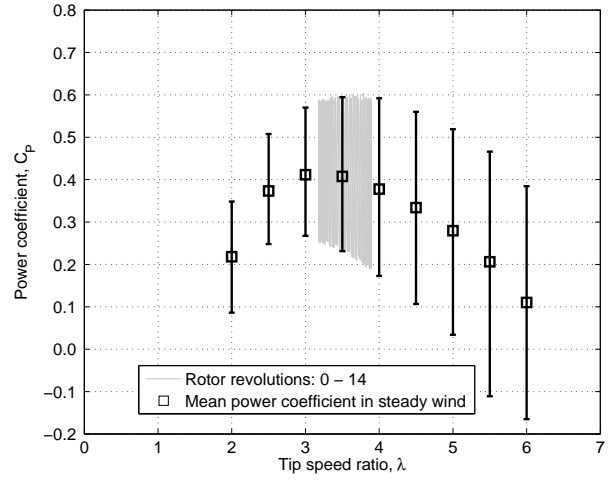


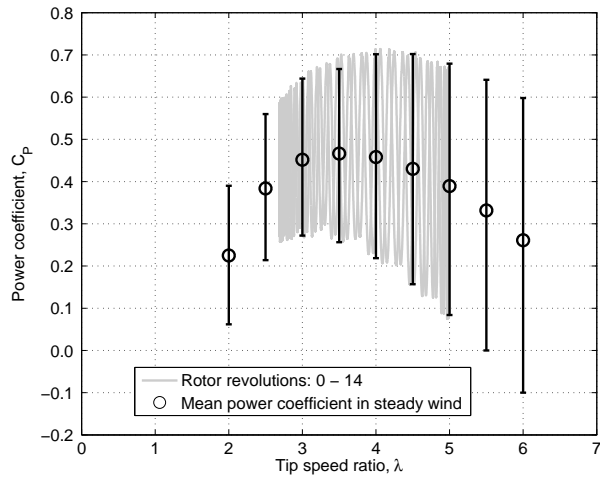
Figure 4: Computed vorticity field surrounding the straight-bladed turbine in **steady** wind conditions, at  $\lambda = 3.5$ , when blade 1 is located at  $\psi = 270^\circ$ . The flow field is represented using contours of vorticity on (a) a vertical plane that contains the axis of rotation of the turbine and that is aligned with the wind direction and (b) a horizontal plane that is perpendicular to the axis of rotation. Figure 4(a) shows contours of the component of vorticity that is perpendicular to the plane, whereas Figure 4(b) shows contours of vorticity magnitude.



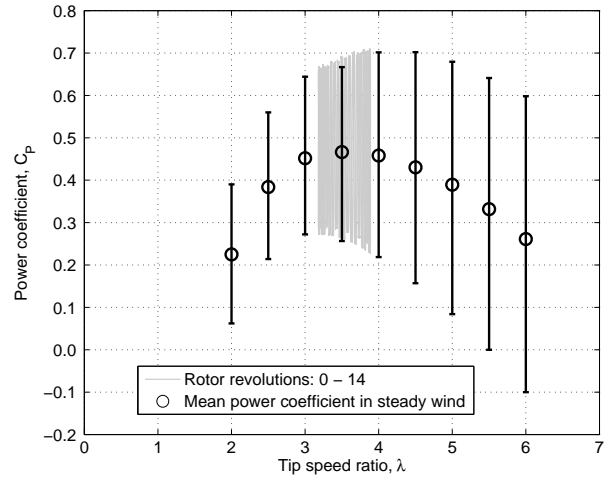
(a) *straight-bladed*,  $\Delta V/V_\infty = \pm 0.3$



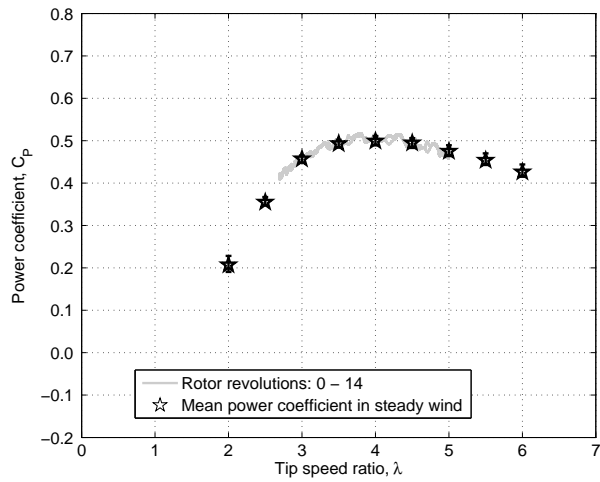
(b) *straight-bladed*,  $\Delta V/V_\infty = \pm 0.1$



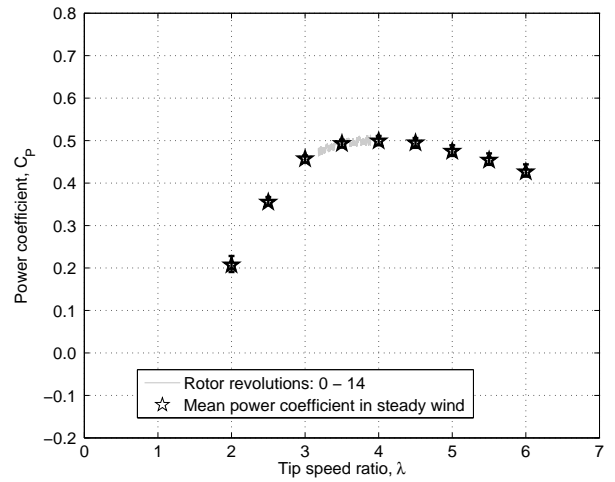
(c) *curved-bladed*,  $\Delta V/V_\infty = \pm 0.3$



(d) *curved-bladed*,  $\Delta V/V_\infty = \pm 0.1$

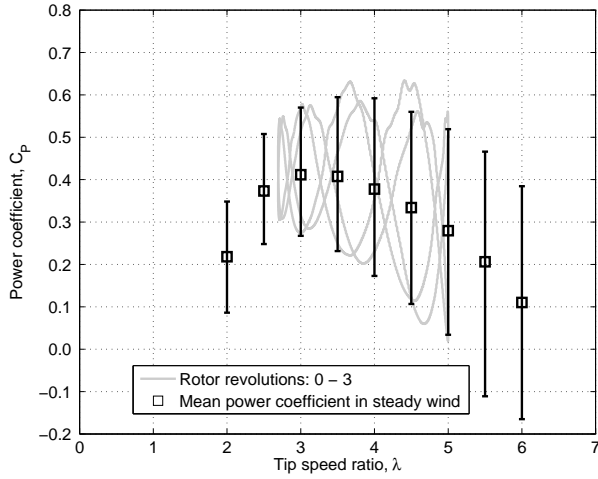


(e) *helically twisted*,  $\Delta V/V_\infty = \pm 0.3$

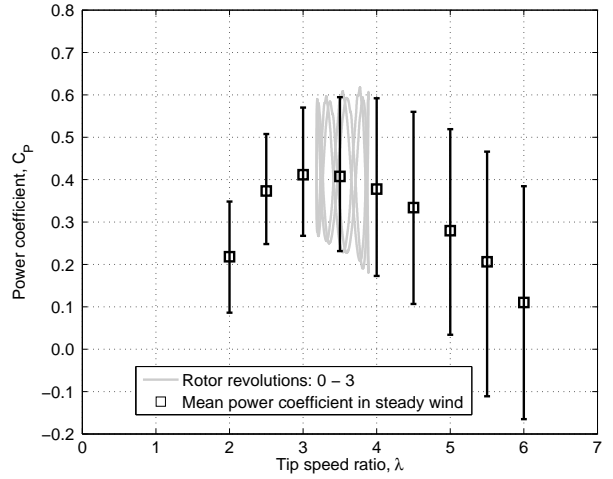


(f) *helically twisted*,  $\Delta V/V_\infty = \pm 0.1$

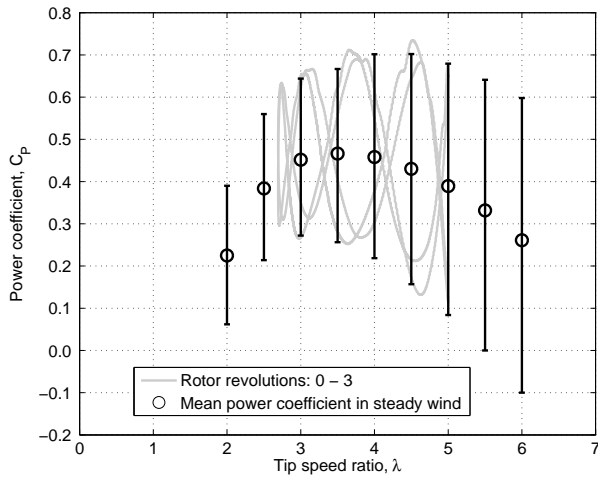
Figure 5: *VTM-predicted variation of the power coefficients for the straight-bladed and curved-bladed turbine and the turbine with helically twisted blades when the rotors were operated at a reduced gust frequency  $k_g = 0.08$  (which corresponds to  $R_g = 14$  at  $\lambda_{mean} = 3.5$ ). Error bars denote the variation of the power coefficient during one rotor revolution in steady wind conditions.*



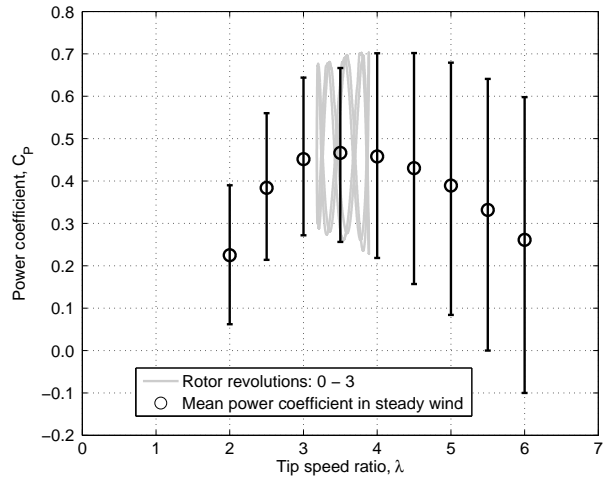
(a) *straight-bladed*,  $\Delta V/V_\infty = \pm 0.3$



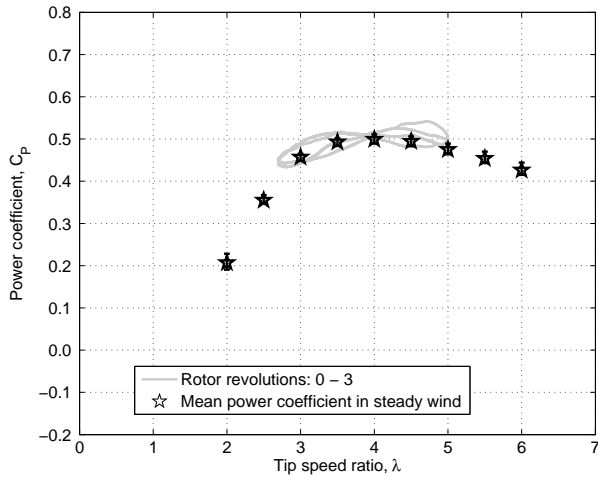
(b) *straight-bladed*,  $\Delta V/V_\infty = \pm 0.1$



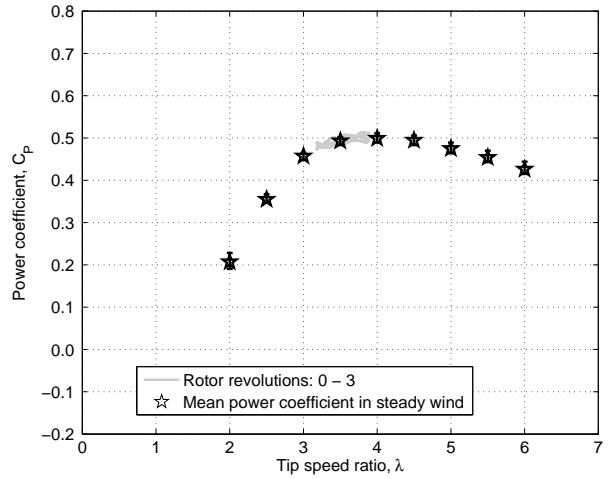
(c) *curved-bladed*,  $\Delta V/V_\infty = \pm 0.3$



(d) *curved-bladed*,  $\Delta V/V_\infty = \pm 0.1$

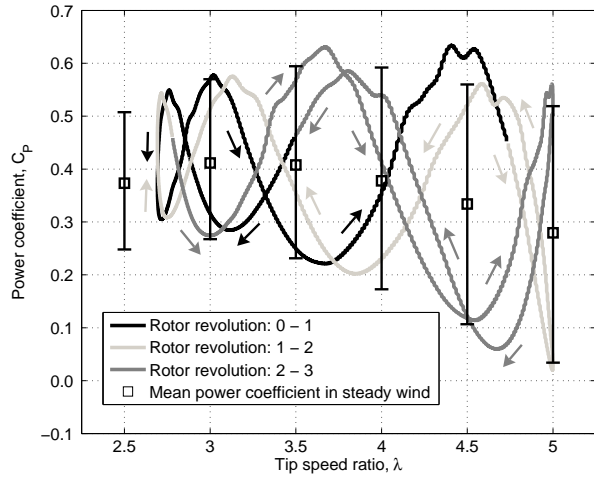


(e) *helically twisted*,  $\Delta V/V_\infty = \pm 0.3$

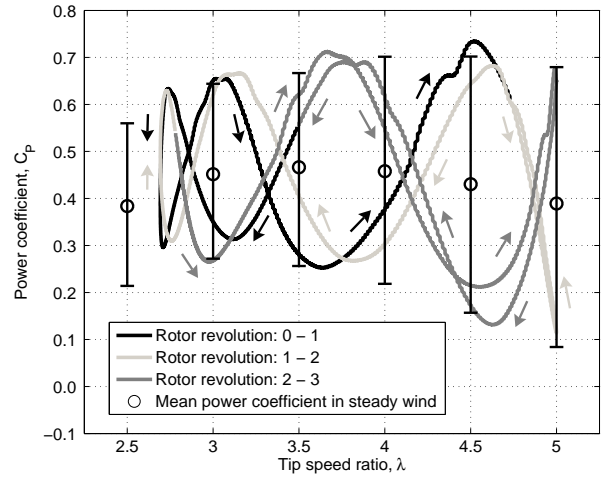


(f) *helically twisted*,  $\Delta V/V_\infty = \pm 0.1$

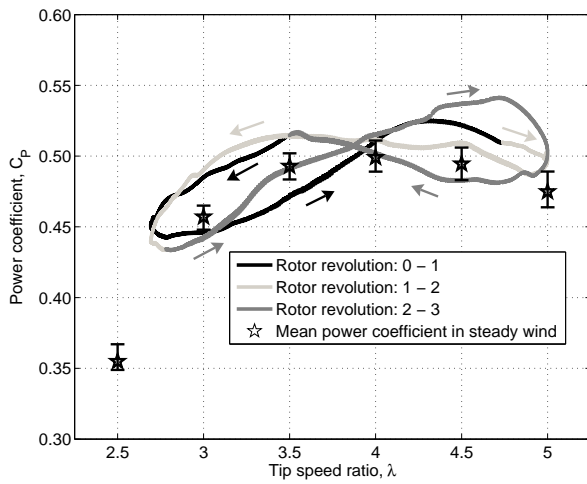
Figure 6: *VTM-predicted variation of the power coefficients for the straight-bladed and curved-bladed turbine and the turbine with helically twisted blades when the rotors were operated at a reduced gust frequency  $k_g = 0.74$  (which corresponds to  $R_g = 1.5$  at  $\lambda_{mean} = 3.5$ ). Error bars denote the variation of the power coefficient during one rotor revolution in steady wind conditions.*



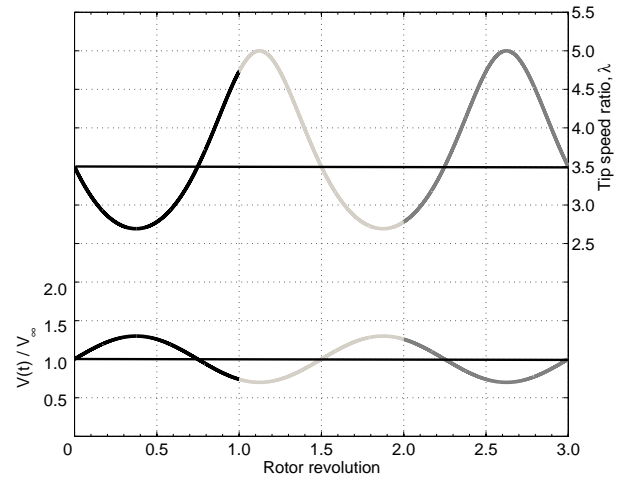
(a) *straight – bladed*



(b) *curved – bladed*



(c) *helically twisted*



(d) *variation of  $V$  and  $\lambda$*

Figure 7: VTM-predicted variation of the power coefficients for the straight-bladed and curved-bladed turbine and the turbine with helically twisted blades when the rotors are operated in unsteady wind conditions with  $\Delta V/V_\infty = \pm 0.3$  and  $R_g = 1.5$  (which corresponds to  $k_g = 0.74$  at  $\lambda = 3.5$ ). Error bars denote the variation of the power coefficient during one rotor revolution in steady wind conditions. Note: the limits of the y-axes in subfigures (a), (b) and (c) are not identical.

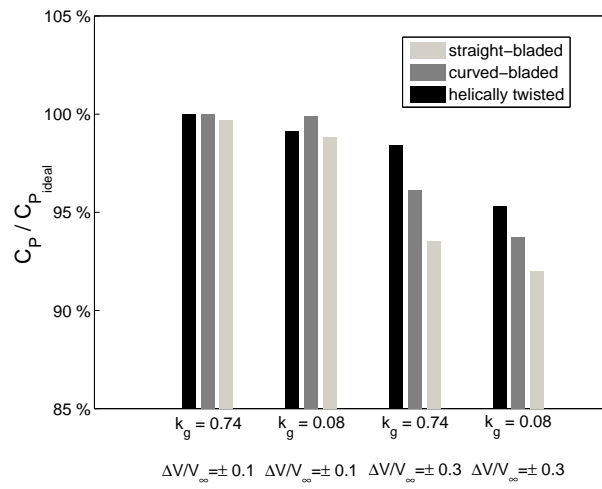
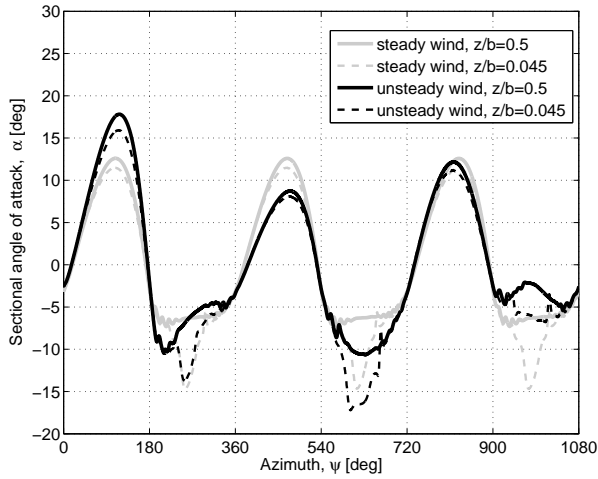
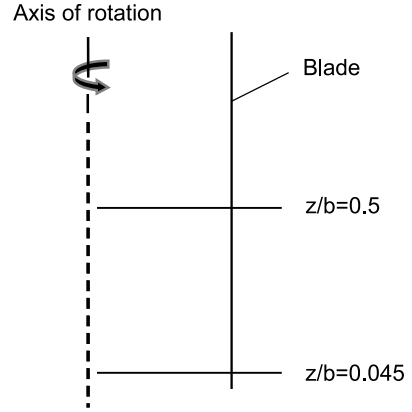


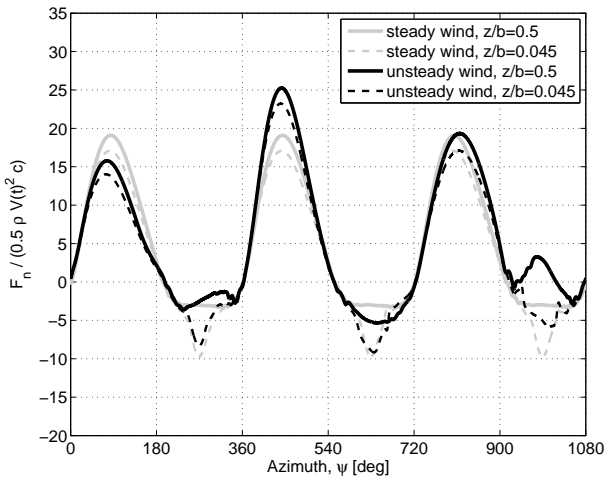
Figure 8: Mean power coefficient produced by the turbine configurations in unsteady wind conditions - as a percentage of that generated by an ‘ideal’ turbine with constant tip speed ratio.



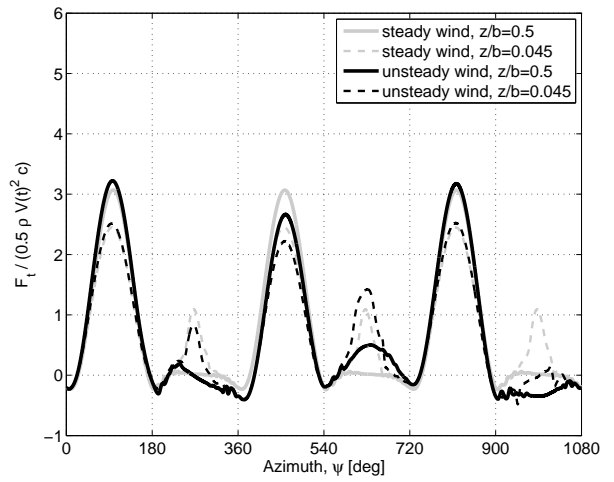
(a) angle of attack



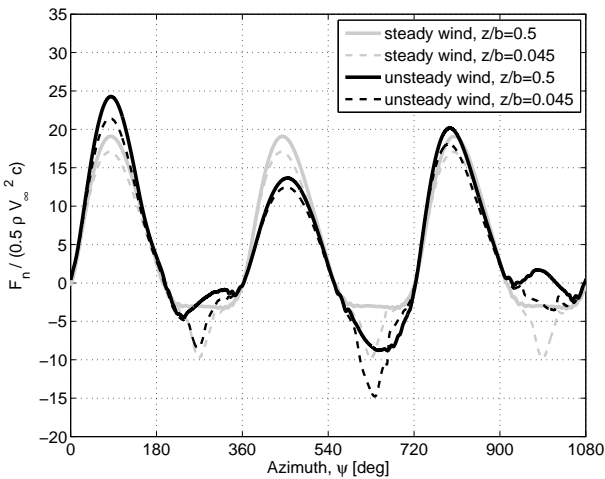
(b) location



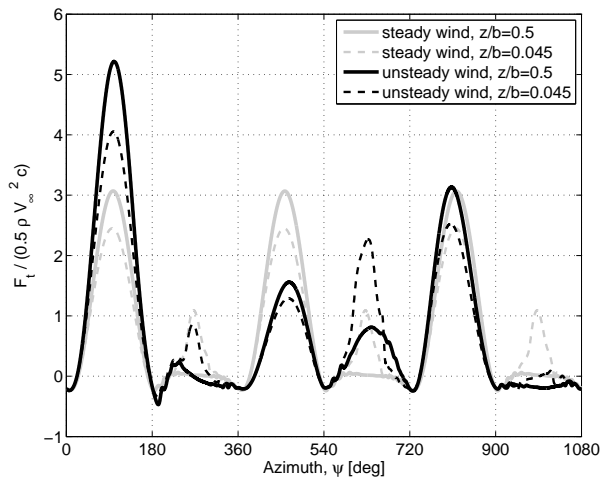
(c) normal force, non - dim. by  $V = V(t)$



(d) tangential force, non - dim. by  $V = V(t)$



(e) normal force, non - dim. by  $V_\infty$



(f) tangential force, non - dim. by  $V_\infty$

Figure 9: VTM-predicted aerodynamic angle of attack and sectional forces in steady and unsteady wind conditions (with  $k_g = 0.74$  and  $\Delta V/V_\infty = \pm 0.3$ ) over three complete rotor revolutions at two different spanwise locations along the reference blade of the straight-bladed turbine.

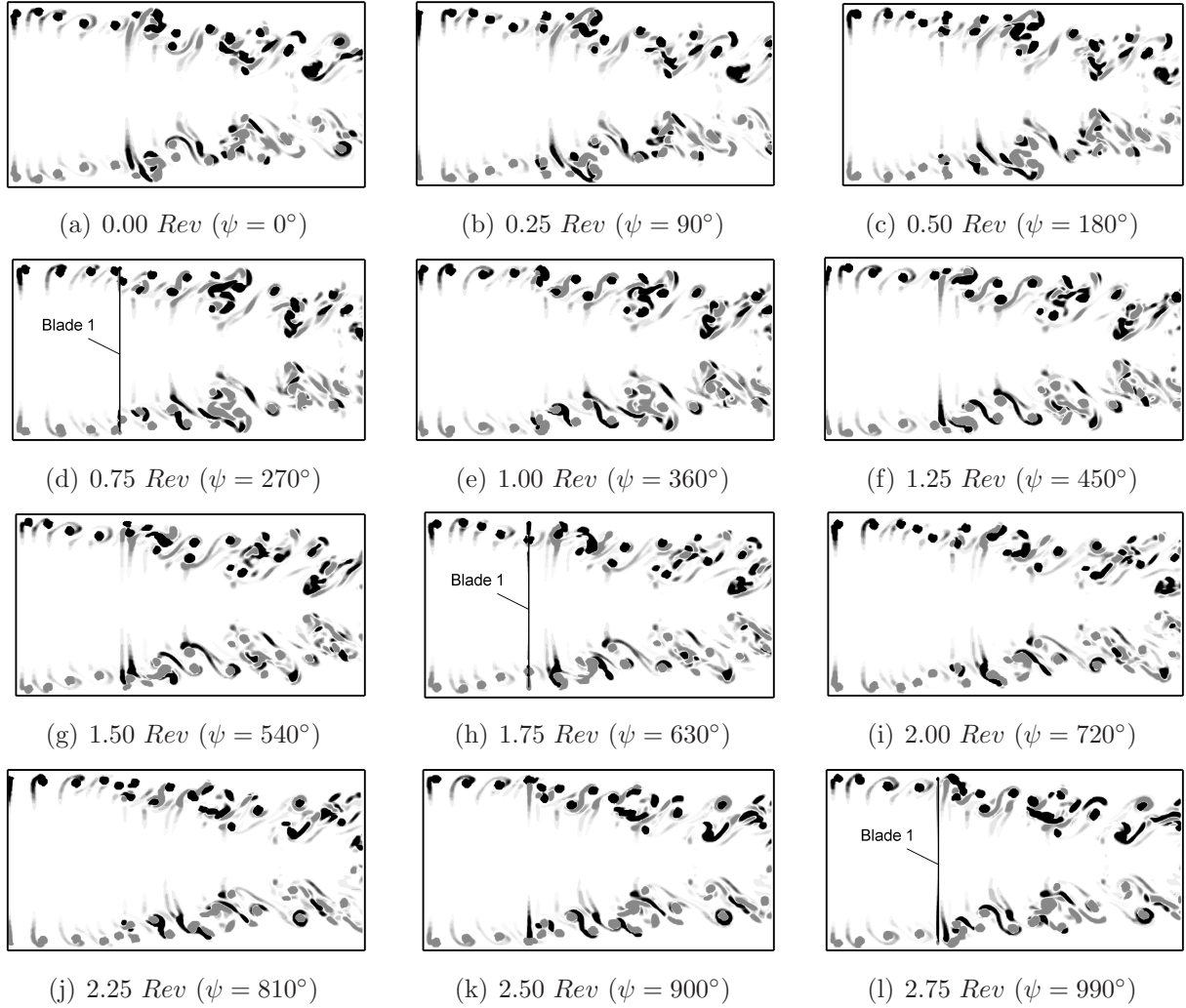


Figure 10: *Computed vorticity field surrounding the straight-bladed turbine in unsteady wind conditions (with  $k_g = 0.74$  and  $\Delta V/V_\infty = \pm 0.3$ ), represented using contours of vorticity on a vertical plane that contains the axis of rotation of the turbine and that is aligned with the wind direction.*

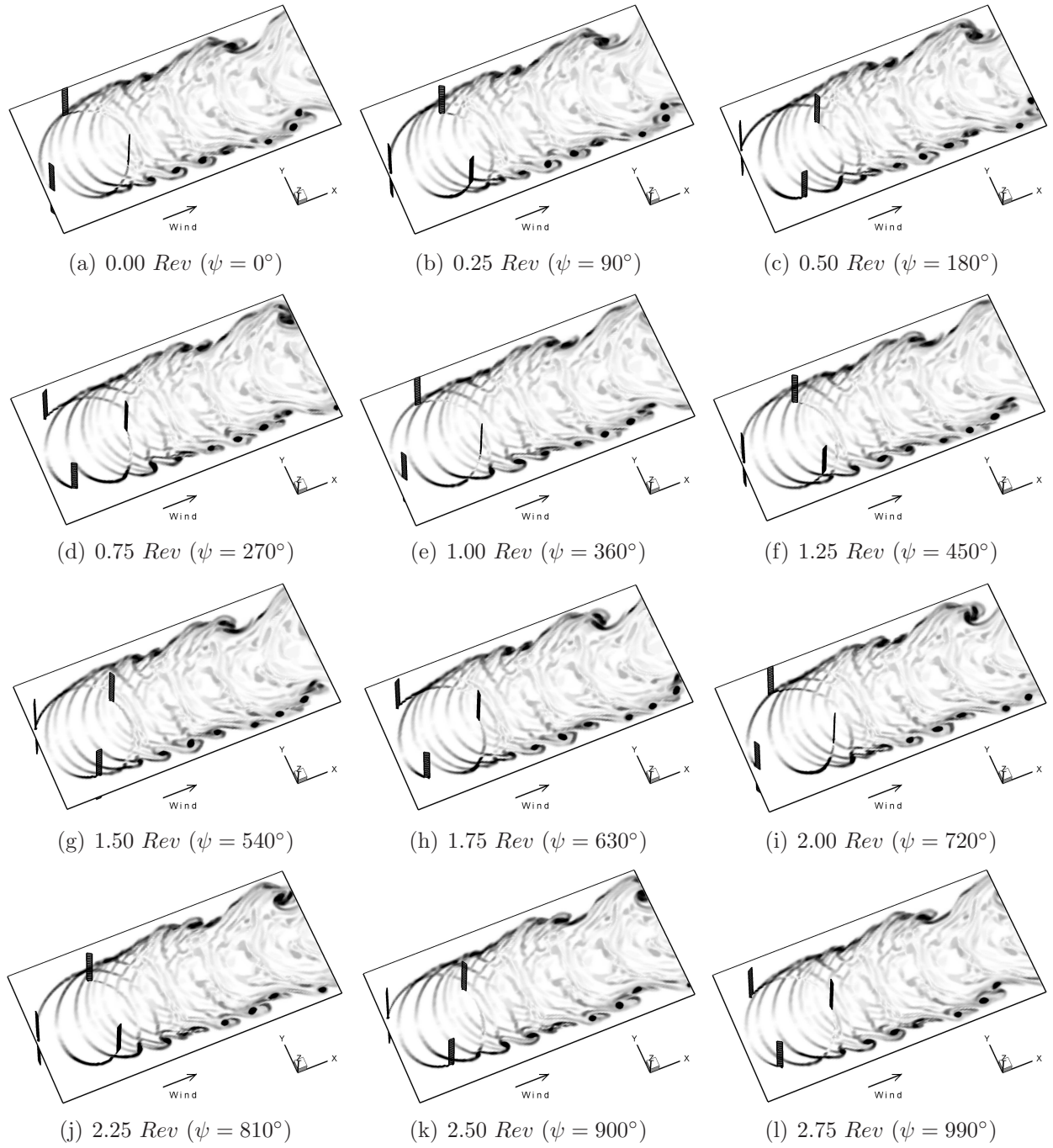


Figure 11: *Computed vorticity field surrounding the straight-bladed turbine in unsteady wind conditions (with  $k_g = 0.74$  and  $\Delta V/V_\infty = \pm 0.3$ ), represented using contours of vorticity on a horizontal plane that is perpendicular to the axis of rotation of the turbine.*



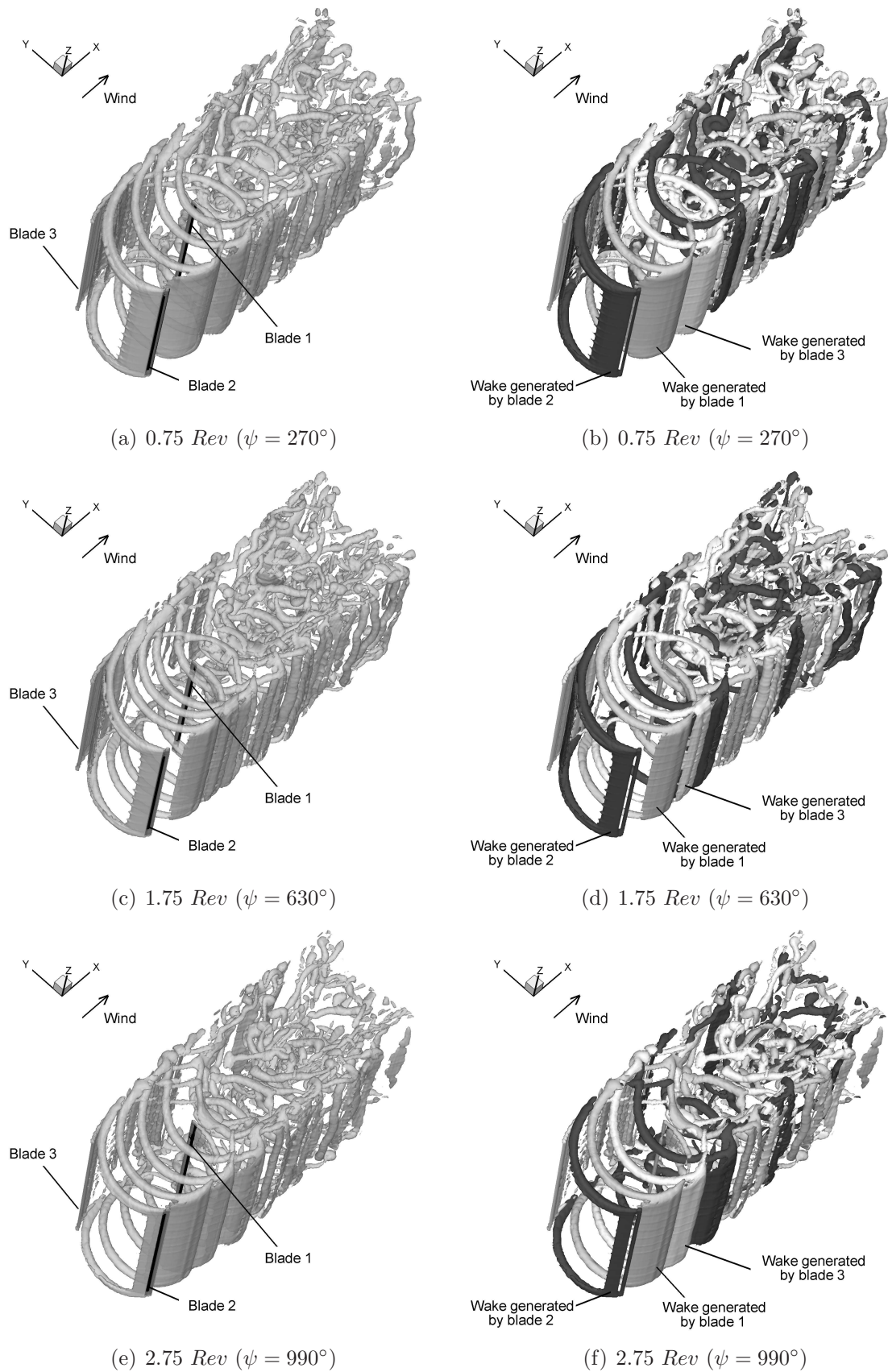


Figure 12: *Computed vorticity field surrounding the straight-bladed turbine in unsteady wind conditions (with  $k_g = 0.74$  and  $\Delta V/V_\infty = \pm 0.3$ ), represented by an isosurface of vorticity. The subfigures (a), (c) and (e) show the entire wake that is generated by the rotor, whereas the different colours in subfigures (b), (d) and (f) represent the vorticity that is developed by the individual blades of the rotor.*